

Article

In Vitro Biocompatibility, Radiopacity, and Physical Property Tests of Nano-Fe₃O₄ Incorporated Poly-L-lactide Bone Screws

Hsin-Ta Wang ^{1,†}, Pao-Chang Chiang ^{2,†}, Jy-Jiunn Tzeng ³, Ting-Lin Wu ³, Yu-Hwa Pan ^{4,5}, Wei-Jen Chang ^{6,7,*} and Haw-Ming Huang ^{6,8,9,*}

¹ School of Organic and Polymeric, National Taipei University of Technology, Taipei 10608, Taiwan; htwang@mail.ntut.edu.tw

² Dental Department, Wan Fang Hospital, Taipei Medical University, Taipei 11696, Taiwan; jumbo117@gmail.com

³ Graduate Institute of Biomedical Materials and Tissue Engineering, College of Biomedical Engineering, Taipei Medical University, Taipei 11031, Taiwan; fungus0429@yahoo.com.tw (J.-J.T.); goku273031@hotmail.com (T.-L.W.)

⁴ Department of General Dentistry, Chang Gung Memorial Hospital, Taipei 10507, Taiwan; shalom.dc@msa.hinet.net

⁵ Chang Gung University, Taoyuan 33371, Taiwan

⁶ School of Dentistry, College of Oral Medicine, Taipei Medical University, Taipei 11031, Taiwan

⁷ Dental Department, Taipei Medical University Shuang-Ho Hospital, New Taipei City 23561, Taiwan

⁸ Graduate Institute of Biomedical Optomechatronics, College of Biomedical Engineering, Taipei 11031, Taiwan

⁹ Ph.D Program in Biotechnology Research and Development, College of Pharmacy, Taipei Medical University, Taipei 11031, Taiwan

* Correspondence: cweijen1@tmu.edu.tw (W.-J.C.); hhm@tmu.edu.tw (H.-M.H.); Tel.: +886-291-937-9783 (W.-J.C. & H.-M.H.)

† Hsin-Ta Wang and Pao-Chang Chiang contributed equally to this work.

Academic Editors: Insung S. Choi and João F. Mano

Received: 18 April 2017; Accepted: 24 May 2017; Published: 26 May 2017

Abstract: The aim of this study was to fabricate biodegradable poly-L-lactic acid (PLLA) bone screws containing iron oxide (Fe₃O₄) nanoparticles, which are radiopaque and 3D-printable. The PLLA composites were fabricated by loading 20%, 30%, and 40% Fe₃O₄ nanoparticles into the PLLA. The physical properties, including elastic modulus, thermal properties, and biocompatibility of the composites were tested. The 20% nano-Fe₃O₄/PLLA composite was used as the material for fabricating the 3D-printed bone screws. The mechanical performance of the nano-Fe₃O₄/PLLA bone screws was evaluated by anti-bending and anti-torque strength tests. The tissue response and radiopacity of the nano-Fe₃O₄/PLLA bone screws were assessed by histologic and CT imaging studies using an animal model. The addition of nano-Fe₃O₄ increased the crystallization of the PLLA composites. Furthermore, the 20% nano-Fe₃O₄/PLLA composite exhibited the highest thermal stability compared to the other Fe₃O₄ proportions. The 3D-printed bone screws using the 20% nano-Fe₃O₄/PLLA composite provided excellent local tissue response. In addition, the radiopacity of the 20% nano-Fe₃O₄/PLLA screw was significantly better compared with the neat PLLA screw.

Keywords: radiopaque polymer; 3D printed bone screw; iron oxide nanoparticles; poly-L-lactic acid

1. Introduction

Metallic bone screws are widely used in the healing of bony defects. Nonetheless, their use requires a second surgical procedure to remove them after healing [1,2]. Additionally, the high elastic

modulus of metallic implants results in stress shielding effect, which leads to a decrease in bone quality and delayed bone healing [3]. Recently, bone screws fabricated with biodegradable polymers were introduced to overcome these problems. Among these biodegradable polymers, polylactic acid (PLA) is commonly used in orthopedic devices, dental rehabilitation, drug delivery, and injectable tissue engineering [4]. One of the advantages of using PLA to fabricate bone implants is that it is easy to shape the bone graft to fit the defect.

Recently, additive manufacturing technologies have been used to manufacture customized scaffolds. Among these technologies, fused deposition modelling (FDM) has been extensively applied for the fabrication of three-dimensional (3D) bio-scaffolds in the biomedical field [5–9]. Previous reports indicate that PLA can be used as an FDM printing material for bone tissue engineering [3,10]. However, using PLA for fabricating bone implants has two disadvantages. First, due to the low mechanical properties, the application of PLA must be limited only at non-weight bearing sites. Second, due to its low specific gravity and electron density, PLA cannot be detected by X-ray radiography [11]. This drawback makes evaluating the degradation and position of PLA devices during placement and healing difficult.

To overcome these problems, researchers began incorporating inorganic materials into the PLA to make composite materials. Fe₃O₄ nanoparticles exhibited excellent osteogenic effects [12–14]. In 2011, De Santis et al. incorporated iron oxide (Fe₃O₄) nanoparticles into poly(ϵ -caprolactone) (PCL) matrix to fabricate magnetic scaffolds. They found that the addition of the Fe₃O₄ nanoparticles increased the elastic modulus of the PCL by 10% [8]. Recently, several researchers added Fe₃O₄ nanoparticles into PLA to fabricate multifunctional biomaterials [15–17]. Although Fe₃O₄ nanoparticles show strong contrast in magnetic resonance imaging (MRI) studies [18], whether or not Fe₃O₄ nanoparticle–PLA composites demonstrate radiopacity is not well studied. In 2015, Huang's group developed an X-ray imaging-enhanced PLA bone screws using Fe₃O₄ nanoparticle–PLA composites [19]. Their results showed that nano-Fe₃O₄/PLLA screws provided better osteogenic properties compared to that of neat PLLA screws. In addition, this material can be used as a 3D printing material. However, the *in vitro* biocompatibility and thermal properties of the material were not discussed in their report.

The aim of this study was to fabricate Fe₃O₄ nanoparticle-PLA bone screws using FDM technology. The local tissue response and *in vitro* calorimetric and mechanical properties of the fabricated screws were evaluated.

2. Materials and Methods

Before the fabrication procedure of the nano-Fe₃O₄/PLLA composite began, the Fe₃O₄ nanoparticles (99.9%, 50 nm, Long Ton, Inc., Taipei, Taiwan) and PLLA powder (molecular weight of 100 kDa, Wei Mon Industry Co., Taipei, Taiwan) were dried at 80 °C overnight. Then, a twin-screw extruder was used to mix the two materials at 150 °C. The extruded nano-Fe₃O₄/PLLA was cooled in a water bath at 25 °C. A pelletizer was used to cut the nano-Fe₃O₄/PLLA composite into small granules. Four nano-Fe₃O₄/PLLA composites containing 0, 20%, 30% and 40% (*w/w*) Fe₃O₄ were manufactured to test for the optimal nano-Fe₃O₄/PLLA ratio for fabricating the bone screws. Three nano-Fe₃O₄/PLLA samples were prepared by injection molding at an injection temperature of 210 °C to test the thermal and biological properties of the composite material. For cell culture tests, nano-Fe₃O₄/PLLA discs with a diameter of 1 cm were fabricated. In addition, 1.65-mm nano-Fe₃O₄/PLLA rods 20 cm in length were also produced to serve as a feeding material for FDM printing.

2.1. Thermal Properties of the Fe₃O₄/PLLA Composites

The thermal properties of the nano-Fe₃O₄/PLLA composites were analyzed using differential scanning calorimetry (DSC) (Q100, TA Instruments, Inc., California, CA, USA). A dried sample (5 mg) under nitrogen flow (50 mL/min) was used. During DSC tests, the samples were heated from 25 to 200 °C at a rate of 10 °C/min. Then, the samples were maintained at 200 °C for 2 min.

During the cooling stage, the samples were cooled from 200 to 30 °C at 10 °C/min and remained at this temperature for 3 min. The heating–cooling scans were performed twice. To reduce the error due to thermal resistance between the composite and the bottom of the DSC crucible and irregular molecular structure in the composite, the glass transition temperature (T_g), cold crystallization temperature (T_c), and melting temperature (T_m) of the samples were determined from the second scan. The thermal stability of the samples was detected using a thermogravimeter (TGA, TG 209 F3 Tarsus, Netzsch, Gerätebau GmbH, Bavarian, Germany). During the tests, 3-mg samples were heated from room temperature to 900 °C at a rate of 20 °C/min. The thermal decomposition temperatures (T_{onset}) and the degradation peak temperature (T_{peak}) were reduced.

2.2. In Vitro Biocompatibility Tests of the Fe_3O_4 /PLLA Composites

To test the in vitro biocompatibility of Fe_3O_4 /PLLA composites, MG63 osteoblast-like cells were cultured on injection molded Fe_3O_4 /PLLA discs that were placed in 24-well culture plates at a density of 1×10^4 cells/well. The cells were cultured in Dulbecco's Modified Eagle's Medium (DMEM; HyClone, Logan, UT, USA) with 10% fetal bovine serum, 4 mM L-glutamine, and 1% penicillin–streptomycin. The discs were cultured in 5% CO_2 at 37 °C and 100% humidity for 1–4 days. The cell viability was determined by staining with MTT (3-[4,5-dimethyl-thiazol-2-yl]-2,5-diphenyltetrazolium bromide) reagent (MTT kit; Roche Applied Science, Mannheim, Germany). The optical absorbance measured at the wavelengths of 570/690 nm in a microplate reader (Model 2020, Anthos Labtec Instruments, Eugendorf, Wals, Austria) was used to determine the cell viability.

2.3. Fabrication of Nano- Fe_3O_4 /PLLA Bone Screws

The screws designed and 3D printed in this study were 3.1 mm in diameter and 12 mm in length with a self-tapping tip. The thread width was 0.3 mm. The geometry of the screw model was established using commercial software (Solidworks, Inc., Waltham, MA, USA). The meshed model was imported into 3D printing software (ReplicatorG 0037, Makerbot, NY, USA) and transferred to the G-code format (Skenforge, Makerbot, NY, USA). As shown in Figure 1, a fused deposition modeling (FDM) machine (Born One, Wanwall, Honk Kong, China) was used to fabricate nano- Fe_3O_4 /PLLA bone screws. The printing thickness was 0.15 mm for each layer. The injection molded nano- Fe_3O_4 /PLLA rods were fed into the extraction nozzle at an extrusion temperature of 185 °C. During the physical property tests, we found that the nano- Fe_3O_4 /PLLA composite with mix ratios greater than 20% significantly decreased the thermal stability of the PLLA. Thus, only 20% nano- Fe_3O_4 /PLLA bone screws were fabricated and used in the following experiments. For all the tests, neat PLLA screws were used as the control group.

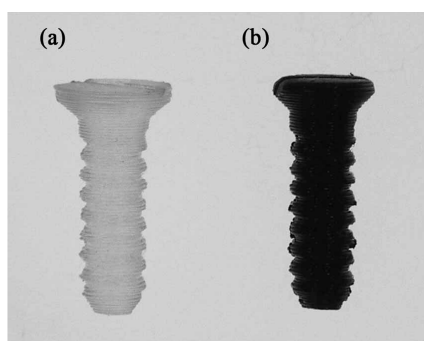


Figure 1. FDM fabricated bone screws using (a) neat PLLA and (b) 20% nano- Fe_3O_4 /PLLA composites.

2.4. Mechanical Tests of the Bone Screws

To test the mechanical strength of the FDM-made nano-Fe₃O₄/PLLA bone screws, the ultimate anti-torque strength and bending strength of the screws were evaluated. According to previous studies [20,21], solid-rigid polyurethane form bone blocks (Sawbones Pacific Research Laboratories Inc., Washington, WA, USA) were used as simulated bone. The simulated bone blocks were cut into cubic units (1 cm × 2 cm × 2 cm). For each bone block specimen, pilot holes (2.5 mm in diameter) were prepared using a drill with the same diameter as the bone screw. After cavity preparation, the fabricated bone screws were screwed into the simulated bone blocks. Before testing, the samples were clamped onto a clamp stand. The peak anti-torque strength of the screws was averaged from the measurements of five samples using a digital torque meter (TQ-8800, Lulton Electronic Enterprise, Taipei, Taiwan).

For the bending strength test, the screw/simulated bone samples were mounted on a custom-designed holding stage and rigidly fixed on the base plate of the universal testing machine (AGS-1000D, Shimadzu, Tokyo, Japan). As shown in Figure 2, the test screws were 90° off the axis to produce a bending force on the samples. A vertical pre-load of 0.5 mm was directly applied to the screw by a force head before testing. Then, the force was applied downward at a rate of 0.05 mm/s until the samples fractured. Five specimens were tested, and for each, the maximum applied load was recorded. The average value of the maximum applied load causing each tested sample to fail was defined as the “bending strength”. For all the mechanical tests, neat PLLA screws served as controls.

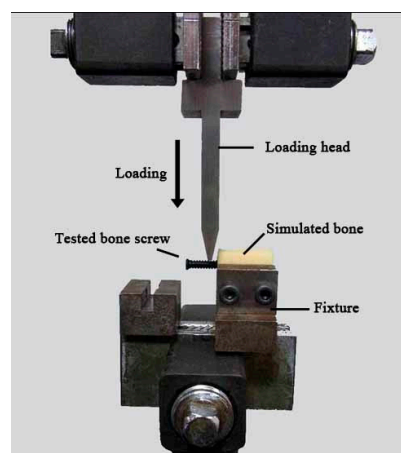


Figure 2. Schematic setup of the bending strength test.

2.5. Animal Experiments

The Institutional Animal Care and Use Committee approved the protocols for all of the animal testing performed in this study (LAC-2014-0123). Three New Zealand white rabbits aged eight months and weighing 3.0–3.5 kg were used as subjects. For each rabbit, one 20% nano-Fe₃O₄/PLLA bone screw was implanted in the left femoral condyle while a neat PLLA screw (control) was implanted in the right leg of the rabbits. Before the bone screw operations, the animal received intramuscular injection (15 mg/kg tiletamine-zolazepam) (Zoletil 50, Virbac, Carros Cedex, France) for general anesthesia. In addition, 2% epinephrine (1.8 mL) was injected at each femoral condyle for local anesthesia. After the skin incision and muscle dissection, a drilled cavity (2.5 mm in diameter) was prepared at both implant sites.

After the bone screws had been implanted, the muscle and skin were closed with absorbable sutures (Vicryl® 4.0, Ethicon, Somerville, NJ, USA). To control pain and reduce the risk of infection, antibiotics were intramuscularly administered for three consecutive days. The animals were killed four weeks post-surgery using a humane method.

The femoral condyles with the bone screws were excised and fixed in 10% formalin. Micro-computed tomographic (micro-CT) images of the bone samples were taken at an energy level of 55 kV at 181 A (Skyscan 1076, Skyscan, Antwerp, Belgium) to determine the radiopacity of the nano-Fe₃O₄/PLLA screws. After micro-CT examination, histomorphometric observation was performed using the same bone blocks. Demineralization was done according to the method of Ayukawa et al. 1998. The bone blocks were cut with a diamond blade saw into 2 mm slices [22]. After dehydration, the slices were embedded in paraffin wax, and 10 µm sections were prepared using an ultramicrotome (Bright 5040, Bright Instrument, Cambs, UK). For histological examination, the specimens were stained with hematoxylin and eosin and observed using a light microscope (CH2, Nikon, Tokyo, Japan) equipped with a digital camera (Coolpix 950, Nikon, Tokyo, Japan) [23].

2.6. Statistical Analysis

Differences in elastic modulus and cell viability between the nano-Fe₃O₄/PLLA composites with various mix ratios were tested using one-way analysis of variance. For the mechanical tests of the fabricated bone screws, Student's *t*-test was used to examine the differences in anti-torque strength and bending strength between the neat PLLA screws and the 20% nano-Fe₃O₄/PLLA screws. Probability values less than 0.05 were considered significant.

3. Results

Figure 3 shows the DSC thermograms recorded for the nano-Fe₃O₄/PLLA composites. The thermograms of the samples showed no significant glass transition. Table 1 shows that the crystallization temperature (*T_c*) of the PLLA composites mixed with various amounts of nano-Fe₃O₄ particles (103–109 °C) was lower than that of neat PLA (117.1 °C). That is, the nano-Fe₃O₄/PLLA composite started to crystallize before the neat PLLA. Additionally, thermograms of the neat PLLA display marked double melting peaks at 162.3 and 167.9 °C for the first and second melting peaks, respectively. As the nano-Fe₃O₄/PLLA mix ratio increased, the double melting peak changed to a single melting peak. The high-temperature melting peak of nano-Fe₃O₄/PLLA composites did not shift with increasing mix ratio.

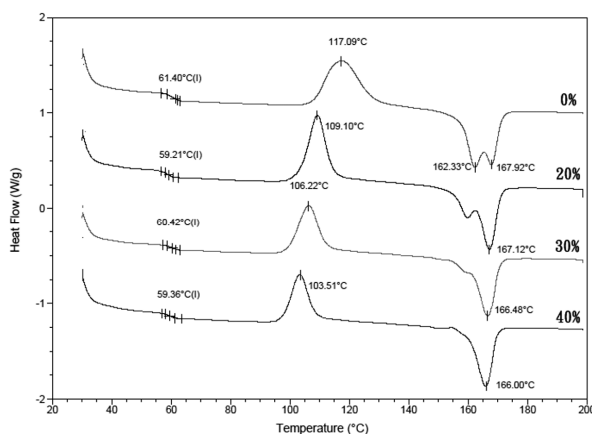


Figure 3. DSC thermograms of the four nano-Fe₃O₄/PLLA composites with various nano-Fe₃O₄/PLLA ratios.

Table 1. Thermal properties of nano-Fe₃O₄/PLLA composites.

Fe ₃ O ₄ (%)	<i>T_g</i>	<i>T_c</i>	<i>T_m</i>	<i>T_{onset}</i>	<i>T_{peak}</i>
0%	61.4	117.1	167.9	309.0	363.9
20%	59.2	109.1	167.1	317.7	338.2
30%	60.4	106.2	166.5	314.6	325.0
40%	59.4	103.5	166	311.9	320.4

Figure 4 illustrates the thermography of the nano-Fe₃O₄/PLLA composites. The addition of 20% nano-Fe₃O₄ particles to the PLLA improved the thermal stability of the polymer (Table 1). The initial decomposition temperature (T_{onset}) of the neat PLLA was 309.0 °C, which rose to 317.7 °C when 20% nano-Fe₃O₄ particles were added. However, it decreased to 314.6 and 311.9 °C when the mix ratios were 30% and 40%, respectively. The presence of nano-Fe₃O₄ particles reduced the degradation peak temperature (T_{peak}). For the neat PLLA, the T_{peak} was recorded as 363.9 °C. T_{peak} was 338.2 °C for the 20% nano-Fe₃O₄/PLLA composite, 325.0 °C for the 30% composite, and 320.4 °C for the 40% nano-Fe₃O₄/PLLA composite.

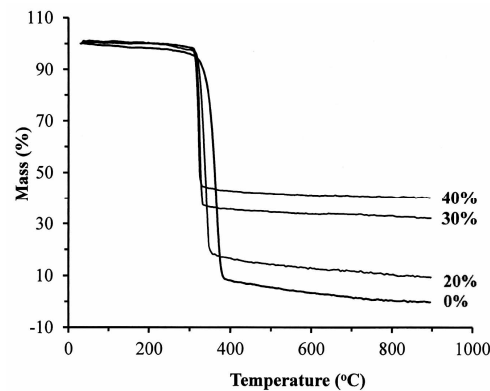


Figure 4. TGA patterns of the four nano-Fe₃O₄/PLLA composites with various nano-Fe₃O₄/PLLA ratios.

MG63 osteoblast-like cells were cultured on the Fe₃O₄/PLLA composites for four days to test the biocompatibility of the Fe₃O₄/PLLA composites. Figure 5 illustrates the growth of the MG63 cells seeded on the nano-Fe₃O₄/PLLA composites. The cells demonstrated normal growth curves on all the composites. The cell numbers were increased in both the Fe₃O₄/PLLA composite groups and the neat PLLA group throughout the entire culture period. When comparing cells grown on the nano-Fe₃O₄/PLLA composites with the various nano-Fe₃O₄/PLLA ratios, no statistically significant differences in cell numbers were observed for any counting interval over the four-day period.

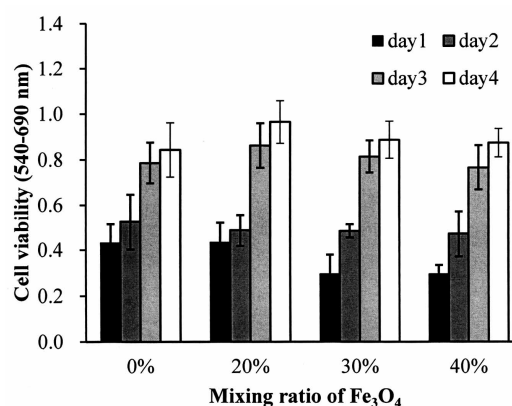


Figure 5. Cell growth assay for MG63 cells seeded onto the nano-Fe₃O₄/PLLA composites and incubated for four days.

In Figure 6a, the bending strength of the neat PLLA bone screw is 20.6 ± 5.9 N. The addition of 20% nano-Fe₃O₄ to the PLLA had no significant effect on the bending strength of the screw. A similar result was obtained in the anti-torque strength experiment. The maximum anti-torque strength of the

neat PLLA was 5.9 ± 1.0 N-cm (Figure 6b). The statistical analysis showed no difference between the neat PLLA and 20% nano-Fe₃O₄/PLLA screws.

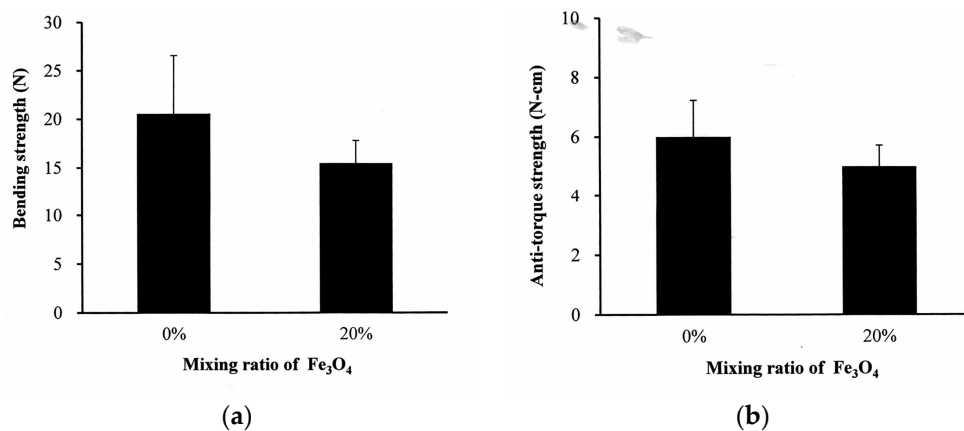


Figure 6. Comparison of (a) bending strength and (b) maximum anti-torque strength between bone screws manufactured with neat PLLA and 20% nano-Fe₃O₄/PLLA composite.

When the bone screws were placed in the rabbits for four weeks, new bone formation at the implant/bone interface was observed both in nano-Fe₃O₄/PLLA group (Figure 7a) and neat PLLA group (Figure 7b). Furthermore, along with the degradation process, bone tissue grew into the nano-Fe₃O₄/PLLA screw at the bone interface between threads. Leached nano-Fe₃O₄/PLLA debris was surrounded by bone tissue without an observable inflammatory response or side effect (Figure 7a). Figure 8 shows typical micro-CT images of the implanted bone screws. The neat PLLA screws showed no radiopacity and could not be distinguished from the surrounding tissue (Figure 8a). However, the addition of 20% nano-Fe₃O₄ particles significantly improved the radiopacity of the PLLA screw. The boundary and location of the 20% nano-Fe₃O₄/PLLA screw were easily identified without any blooming artifact (Figure 8b).

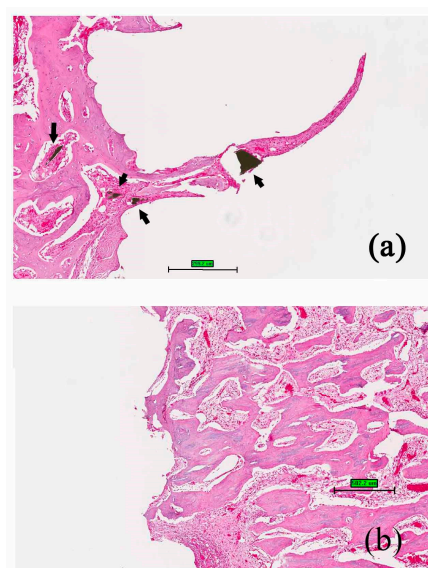


Figure 7. Histology of the bone tissue at the screw/bone interface for (a) 20% nano-Fe₃O₄/PLLA group and (b) neat PLLA group after four weeks of healing. The black arrow indicates debris leached from the nano-Fe₃O₄/PLLA composite, which is surrounded by bone tissue. There is no observable local toxicity in the bone tissue. Black arrows indicate the leached nano-Fe₃O₄/PLLA debris was surrounded by bone tissue. Scale bar: (a) 0.3 mm (b) 0.5 mm.

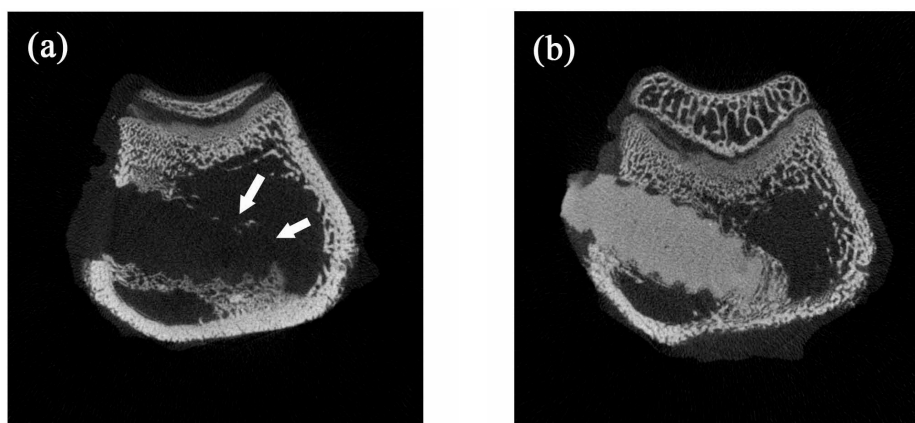


Figure 8. Typical micro-CT images of (a) neat PLLA screw and (b) 20% nano-Fe₃O₄/PLLA screw implanted in rabbit bone. The addition of 20% Fe₃O₄ nanoparticles significantly improved the radiopacity of the PLLA screws.

4. Discussion

We applied an FDM method for 3D printing of nano-Fe₃O₄/PLLA composite bone screws. The screws were produced by extruding the PLLA composite via a heated extrusion nozzle. Thus, the nano-Fe₃O₄/PLLA used in this study was a thermoplastic material with the appropriate viscosity when melted so that it could be extruded from the extrusion nozzle. FDM technology may be used to print poly(ϵ -caprolactone)/Fe₃O₄ [8] and neat PLLA [3] devices directly for tissue engineering. Nonetheless, whether the addition of nano-Fe₃O₄ particles to the PLLA affects their viscosity and 3D printability has not been systematically investigated. Although body temperature is only 36–37 °C, the material may be subjected to a temperature of 185 °C when used for FDM fabrication. Thus the thermal stability of the nano-Fe₃O₄/PLLA composite at such a high temperature was tested in this study. The glass transition temperature is related to the physical properties of the PLLA. The DSC thermograms of the samples (Figure 3) showed no significant shift in glass temperature transition. Thus, the fabricated nano-Fe₃O₄/PLLA composites may be used to manufacture the bone screws using the FDM method (Figure 1).

The crystallization temperature (T_c) was affected by the addition of nano-Fe₃O₄ particles. It is well known that a lower crystallization temperature results in faster crystallization [24]. Thus, the addition of nano-Fe₃O₄ particles into the PLLA reduced the energy required to achieve crystallinity. The melting behavior of PLLA is complex. As shown in Figure 3, the neat PLLA exhibited double melting peaks. This is because PLLA is a semi-crystalline polymer made up of different types of crystals [24,25]. Additionally, the presence of the filler significantly modified the overall crystallinity. The change in the ratio of the first and the second melting peaks of the samples indicates that the nano-Fe₃O₄ particles influence the size of the crystals. The low-temperature melting peak of the PLLA composites increased with the increasing nano-Fe₃O₄/PLLA ratio. It is because the increase in nano-Fe₃O₄ makes the crystallization of PLLA more complete, and the number of imperfect crystals decreases [26]. Overall, the changes of T_c and T_m (Figure 3 and Table 1) indicate that the nano-Fe₃O₄ particles act as a nucleating agent to enhance the crystallization rate [24,27]. This improves the perfection of the crystals in the PLLA [24,27].

Researchers have added various contrast agents to enhance the radiopacity of polymeric devices. Most investigators reported that these compounds reduced the thermal stability of the polymer [11,28,29]. However, our results showed a different trend. The addition to Fe₃O₄ nanoparticles improving not only the radiopacity of the PLLA (Figure 8b) but also increasing the thermal stability of the polymer. Figure 4 and Table 1 show that the highest decomposition temperatures occurred when 20% Fe₃O₄ nanoparticles were incorporated into the PLLA. This result is consistent with the report

by Rakmae et al. (2011). They found that the addition of filler to the PLLA increased the thermal decomposition temperatures (T_{onset}) of the composite compared with that of the neat polymer [30]. They reported that the thermal stability of the PLLA composite was due to the thermally stable filler, which decreased the decomposition of the polymer. These additives may act as barriers to prevent heat transfer [30]. This improvement also contributes to the interface interaction between the nanoparticles and the PLLA [31]. However, the composites containing 30% or 40% Fe_3O_4 have lower thermal decomposition temperatures than that of 20% samples. It may be due to the decrement of molecular weight during mixing with a higher ratio of inorganic filler [32]. The addition of 20% nano- Fe_3O_4 particles provided the best dispersion and distribution of nano- Fe_3O_4 particles in the PLLA.

The CT image shown in Figure 8b demonstrated that the addition of nano- Fe_3O_4 particles at 20% provided excellent X-ray visibility. These findings are consistent with previous reports that the addition of 20% contrast agent to polymers provided optimal X-ray visibility without altering the physical properties of the polymer [29,33]. Thus, it is reasonable to suggest that the 20% nano- Fe_3O_4 /PLLA has optimal thermal stability as well as radiopacity. However, the bending strength of this composite is still not large enough for use in weight-bearing areas. It only can be used in non-weight-bearing areas.

Although PLLA is a non-toxic, biodegradable material, the biocompatibility of the added contrast agents is still a concern when it leaches into the surrounding tissue during the degradation process. For example, BaSO_4 was introduced as the contrast agent for increasing the radiopacity of bone cement. However, it was reported that BaSO_4 induced osteolysis [28]. Figure 7 shows the osteoblastic cells cultured on the surfaces of the nano- Fe_3O_4 /PLLA discs. The cells demonstrated normal morphology and growth curves. When the material was 3D printed to make the screw and implanted into the tibia of the rabbits, bone tissue growth into the screw was observed (Figure 7). The leached nano- Fe_3O_4 /PLLA was found in the bone marrow as well as at the screw-bone interface. No adverse effects on the rabbit bone tissue were found. Thus, the nano- Fe_3O_4 /PLLA composite was safe for use as an implant. However, the animal study was performed for only four weeks, the long-term systemic toxicity and inflammation response due to hydrolysis of this PLLA screw cannot be determined. This is the limitation of the current study. In addition, to reduce the toxicity and inflammation response, lower amounts of iron oxide nanoparticles and iron oxide nanoparticles coated with a biocompatible polymer shell [8] can also be considered to incorporate into PLLA polymer.

5. Conclusions

In conclusion, the 20% nano- Fe_3O_4 /PLLA bone screw fabricated in this study demonstrated good biocompatibility, physical, and radiopacity properties. It can be a potential material for fabricating 3D-printed bone screws with radiopacity. These results may serve as a useful reference for future advanced studies of such composites.

Acknowledgments: This study was supported by grants from Taipei Medical University and the National Taipei University of Technology, Taipei, Taiwan (USTP-NTUT-TMU-104-10).

Author Contributions: Wei-Jen Chang and Haw-Ming Huang conceived and designed the experiments; Jy-Jiunn Tzeng and Ting-Lin Wu performed the experiments; Hsin-Ta Wang and Pao-Chang Chiang analyzed the data and wrote the paper; Yu-Hwa Pan contributed reagents, materials, and analysis tools.

Conflicts of Interest: The authors declare no conflict of interest.

References

1. Temenoff, J.S.; Mikos, A.G. Injectable biodegradable materials for orthopaedic tissue engineering. *Biomaterials* **2000**, *21*, 2405–2412. [[CrossRef](#)]
2. Jackson, D.W.; Simon, T.M. Tissue engineering principles in orthopaedic surgery. *Clin. Orthop. Relat. Res.* **1999**, *367*, S31–S45. [[CrossRef](#)]
3. Giordano, R.A.; Wu, B.M.; Borland, S.W.; Cima, L.G.; Sachs, E.M.; Cima, M.J. Mechanical properties of dense polylactic acid structures fabricated by three dimensional printing. *J. Biomater. Sci. Polym. Ed.* **1996**, *8*, 63–75. [[CrossRef](#)] [[PubMed](#)]

4. Lei, K.; Shen, W.; Cao, L.; Yu, L.; Ding, J. An injectable thermogel with high radiopacity. *Chem. Commun.* **2015**, *51*, 6080–6083. [[CrossRef](#)] [[PubMed](#)]
5. Puppi, D.; Mota, C.; Gazzarri, M.; Dinucci, D.; Gloria, A.; Myrzabekova, M.; Ambrosio, L.; Chiellini, F. Additive manufacturing of wet-spun polymeric scaffolds for bone tissue engineering. *Biomed. Microdevices* **2012**, *14*, 1115–1127. [[CrossRef](#)] [[PubMed](#)]
6. Mota, C.; Puppi, D.; Dinucci, D.; Errico, C.; Bártolo, P.; Chiellini, F. Dual-scale polymeric constructs as scaffolds for tissue engineering. *Materials* **2011**, *4*, 527–542. [[CrossRef](#)]
7. Khalil, S.; Nam, J.; Sun, W. Multi-nozzle deposition for construction of 3D biopolymer tissue scaffolds. *Rapid Prototyp. J.* **2005**, *11*, 9–17. [[CrossRef](#)]
8. De Santis, R.; Gloria, A.; Russo, T.; D’Amora, U.; Zepetelli, S.; Dionigi, C.; Sytcheva, A.; Herrmannsdörfer, T.; Dediu, V.; Ambrosio, L. A basic approach toward the development of nanocomposite magnetic scaffolds for advanced bone tissue engineering. *J. Appl. Polym. Sci.* **2011**, *122*, 3599–3605. [[CrossRef](#)]
9. De Santis, R.; Gloria, A.; Russo, T.; D’Amora, U.; D’Antò, V.; Bollino, F.; Catauro, M.; Mollica, F.; Rengo, S.; Ambrosio, L. Advanced composites for hard-tissue engineering based on PCL/organic–inorganic hybrid fillers: from the design of 2D substrates to 3D rapid prototyped scaffolds. *Polym. Compos.* **2013**, *34*, 1413–1417. [[CrossRef](#)]
10. Bose, S.; Vahabzadeh, S.; Bandyopadhyay, A. Bone tissue engineering using 3D printing. *Mater. Today* **2013**, *16*, 496–504. [[CrossRef](#)]
11. James, N.R.; Philip, J.; Jayakrishnan, A. Polyurethanes with radiopaque properties. *Biomaterials* **2006**, *27*, 160–166. [[CrossRef](#)] [[PubMed](#)]
12. Wu, Y.; Jiang, W.; Wen, X.; He, B.; Zeng, X.; Wang, G.; Gu, Z. A novel calcium phosphate ceramic-magnetic nanoparticle composite as a potential bone substitute. *Biomed. Mater.* **2010**, *5*, 15001. [[CrossRef](#)] [[PubMed](#)]
13. Meng, J.; Zhang, Y.; Qi, X.; Kong, H.; Wang, C.; Xu, Z.; Xie, S.; Gu, N.; Xu, H. Paramagnetic nanofibrous composite films enhance the osteogenic responses of pre-osteoblast cells. *Nanoscale* **2010**, *2*, 2565–2569. [[CrossRef](#)] [[PubMed](#)]
14. Shan, D.; Shi, Y.; Duan, S.; Wei, Y.; Cai, Q.; Yang, X. Electrospun magnetic poly(L-lactide) (PLLA) nanofibers by incorporating PLLA-stabilized Fe₃O₄ nanoparticles. *Mater. Sci. Eng. C* **2013**, *33*, 3498–3505. [[CrossRef](#)] [[PubMed](#)]
15. Xu, B.; Dou, H.; Tao, K.; Sun, K.; Ding, J.; Shi, W.; Guo, X.; Li, J.; Zhang, D.; Sun, K. “Two-in-One” fabrication of Fe₃O₄/MePEG–PLA composite nanocapsules as a potential ultrasonic/MRI dual contrast agent. *Langmuir* **2011**, *7*, 12134–12142. [[CrossRef](#)] [[PubMed](#)]
16. Wei, Q.; Li, T.; Wang, G.; Li, H.; Qian, Z.; Yang, M. Fe₃O₄ nanoparticles-loaded PEG–PLA polymeric vesicles as labels for ultrasensitive immunosensors. *Biomaterials* **2010**, *31*, 7332–7339. [[CrossRef](#)] [[PubMed](#)]
17. Shen, L.K.; Fan, K.H.; Wu, T.L.; Huang, H.M.; Leung, T.K.; Chen, C.J.; Chang, W.J. Fabrication and magnetic testing of a poly-L-lactide biocomposite incorporating magnetite nanoparticles. *J. Polym. Eng.* **2014**, *34*, 237–240. [[CrossRef](#)]
18. Baumgartner, J.; Bertinetti, L.; Widdrat, M.; Hirt, A.M.; Faivre, D. Formation of magnetite nanoparticles at low temperature: From superparamagnetic to stable single domain particles. *PLoS ONE* **2013**, *8*, e5707. [[CrossRef](#)] [[PubMed](#)]
19. Chang, W.J.; Pan, Y.H.; Tzeng, J.J.; Wu, T.L.; Fong, T.H.; Feng, S.W.; Huang, H.M. Development and testing of X-ray imaging-enhanced poly-L-lactide bone screws. *PLoS ONE* **2015**, *10*, e0140354. [[CrossRef](#)] [[PubMed](#)]
20. Hong, J.; Lim, Y.J.; Park, S.O. Quantitative biomechanical analysis of the influence of the cortical bone and implant length on primary stability. *Clin. Oral. Implants Res.* **2012**, *23*, 1193–1197. [[CrossRef](#)] [[PubMed](#)]
21. Hsu, J.T.; Fuh, L.J.; Tu, M.G.; Li, Y.F.; Chen, K.T.; Huang, H.L. The effects of cortical bone thickness and trabecular bone strength on noninvasive measures of the implant primary stability using synthetic bone models. *Clin. Implant Dent. Relat. Res.* **2013**, *15*, 251–261. [[CrossRef](#)] [[PubMed](#)]
22. Ayukawa, Y.; Takeshita, F.; Inoue, T.; Yoshinari, M.; Shimono, M.; Suetsugu, T.; Tanaka, T. An immunoelectron microscopic localization of noncollagenous bone proteins (osteocalcin and osteopontin) at the bone-titanium interface of rat tibiae. *J. Biomed. Mater. Res.* **1998**, *41*, 111–119. [[CrossRef](#)]
23. Xiang, W.; Baolin, L.; Yan, J.; Yang, X. The effect of bone morphogenetic protein on osseointegration of titanium implants. *J. Oral. Maxillofac. Surg.* **1993**, *51*, 647–651. [[CrossRef](#)]

24. Cipriano, T.F.; da Silva, A.L.N.; da Silva, A.H.M.; da Fonseca Thomé de Sousa, A.M.F.; da Silva, G.M.; Rocha, M.G. Thermal, rheological and morphological properties of poly (Lactic Acid) (PLA) and talc composites. *Polímeros* **2014**, *24*, 276–282.
25. Gregorova, A.; Sedlarik, V.; Pastorek, M.; Jachandra, H.; Stelzer, F. Effect of compatibilizing agent on the properties of highly crystalline composites based on poly(lactic acid) and wood flour and/or mica. *J. Polym. Environ.* **2011**, *19*, 372–381. [[CrossRef](#)]
26. Cai, T.H. Crystallization and melting behavior of biodegradable poly(L-lactic acid)/talc composites. *J. Chem.* **2012**, *9*, 1569–1574. [[CrossRef](#)]
27. Suryanegara, L.; Nakagaito, A.N.; Yano, H. The effect of crystallization of PLA on the thermal and mechanical properties of microfibrillated cellulose-reinforced PLA composites. *Compos. Sci. Technol.* **2009**, *69*, 1187–1192. [[CrossRef](#)]
28. Aldenhoff, Y.B.; Kruft, M.A.; Pijpers, A.P.; van der Veen, F.H.; Bulstra, S.K.; Kuijjer, R.; Koole, L.H. Stability of radiopaque iodine-containing biomaterials. *Biomaterials* **2002**, *23*, 881–886. [[CrossRef](#)]
29. Kiran, S.; James, N.R.; Jayakrishnan, A.; Joseph, R. Polyurethane thermoplastic elastomers with inherent radiopacity for biomedical applications. *J. Biomed. Mater. Res. A* **2012**, *100*, 3472–3479. [[CrossRef](#)] [[PubMed](#)]
30. Rakmae, S.; Ruksakulpiwat, Y.; Sutapun, W.; Suppakarn, N. Effects of mixing technique and filler content on physical properties of bovine bone-based CHA/PLA composites. *J. Appl. Polym. Sci.* **2011**, *122*, 2433–2441. [[CrossRef](#)]
31. Albano, C.; Gonzalez, G.; Palacios, J.; Karam, A.; Covis, M. PLLA–HA vs. PLGA–HA characterization and comparative analysis. *Polym. Compos.* **2013**, *34*, 1433–1442. [[CrossRef](#)]
32. Liu, X.; Wang, T.; Chow, L.C.; Yang, M.; Mitchell, J.W. Effects of inorganic fillers on the thermal and mechanical properties of poly(lactic acid). *Int. J. Polym. Sci.* **2014**, *2014*, 827028. [[CrossRef](#)] [[PubMed](#)]
33. Coutu, J.M.; Fatimi, A.; Berrahmoune, S.; Soulez, G.; Lerouge, S. A new radiopaque embolizing agent for the treatment of endoleaks after endovascular repair: Influence of contrast agent on chitosan thermogel properties. *J. Biomed. Mater. Res. B* **2013**, *101*, 153–161. [[CrossRef](#)] [[PubMed](#)]



© 2017 by the authors. Licensee MDPI, Basel, Switzerland. This article is an open access article distributed under the terms and conditions of the Creative Commons Attribution (CC BY) license (<http://creativecommons.org/licenses/by/4.0/>).